AFRL-ML-WP-TP-2006-420

STRUCTURAL HEALTH MONITORING OF AN AIRCRAFT PANEL USING CONTINUOUS AE SENSOR (PREPRINT)

Mannur J. Sundaresan, Gangadhararao Grandhi, and Francis Nkrumah

APRIL 2006

Approved for public release; distribution is unlimited.

STINFO COPY

MATERIALS AND MANUFACTURING DIRECTORATE
AIR FORCE RESEARCH LABORATORY
AIR FORCE MATERIEL COMMAND
WRIGHT-PATTERSON AIR FORCE BASE, OH 45433-7750

NOTICE AND SIGNATURE PAGE

AFRL-ML-WP-TP-2006-420 HAS BEEN REVIEWED AND IS APPROVED FOR PUBLICATION IN ACCORDANCE WITH ASSIGNED DISTRIBUTION STATEMENT.

//Signature//

JUAN G. CALZADA, Project Engineer
Nondestructive Evaluation Branch
Metals, Ceramics & NDE Division

//Signature//

ROBERT T. MARSHALL, Acting Chief
Nondestructive Evaluation Branch
Metals, Ceramics & NDE Division

//Signature//

GERALD J. PETRAK, Assistant Chief
Metals, Ceramics & NDE Division
Materials and Manufacturing Directorate

This report is published in the interest of scientific and technical information exchange, and its publication does not constitute the Government's approval or disapproval of its ideas or findings.

*Disseminated copies will show "//Signature//" stamped or typed above the signature blocks.

REPORT DOCUMENTATION PAGE

Form Approved
OMB No. 0704-0188

1. REPORT DATE *(DD-MM-YY)*	2. REPORT TYPE	3. DATES COVERED *(From - To)*
April 2006	Conference Paper Preprint	02/01/2004 – 09/01/2005

4. TITLE AND SUBTITLE
STRUCTURAL HEALTH MONITORING OF AN AIRCRAFT PANEL USING CONTINUOUS AE SENSOR (PREPRINT)

5a. CONTRACT NUMBER
F33615-03-D-5204-0013

5b. GRANT NUMBER

5c. PROGRAM ELEMENT NUMBER
63112F

6. AUTHOR(S)
Mannur J. Sundaresan, Gangadhararao Grandhi, and Francis Nkrumah

5d. PROJECT NUMBER
43494105

5e. TASK NUMBER
41

5f. WORK UNIT NUMBER
05

7. PERFORMING ORGANIZATION NAME(S) AND ADDRESS(ES)
North Carolina A&T State University
Department of Mechanical and Chemical Engineering
Greensboro, NC 27411

8. PERFORMING ORGANIZATION REPORT NUMBER

9. SPONSORING/MONITORING AGENCY NAME(S) AND ADDRESS(ES)
Materials and Manufacturing Directorate
Air Force Research Laboratory
Air Force Materiel Command
Wright-Patterson AFB, OH 45433-7750

10. SPONSORING/MONITORING AGENCY ACRONYM(S)
AFRL-ML-WP

11. SPONSORING/MONITORING AGENCY REPORT NUMBER(S)
AFRL-ML-WP-TP-2006-420

12. DISTRIBUTION/AVAILABILITY STATEMENT
Approved for public release; distribution is unlimited.

13. SUPPLEMENTARY NOTES
This work, resulting in whole or in part from Department of the Air Force contract F33615-03-D-5204-0013, has been submitted to the 14th International Conference on Composites/Nano Engineering Proceedings. If this work is published, the publisher may assert copyright.

PAO Case Number: AFRL/WS 06-0840, 31 Mar 2006. This paper contains color content.

14. ABSTRACT
Fatigue crack growth during the service of aging aircrafts has become an important issue and the monitoring of such cracks in hot spots is desirable. A structural health monitoring sensor system that uses acoustic emission technique for monitoring safety of such structures is described in this report. A “continuous sensor” formed by connecting multiple sensor nodes in series arrangement to form a single channel sensor is proposed to monitor acoustic emission signals. This report describes the work performed for monitoring fatigue cracks in aluminum lap joints. The traditional AE sensors as well as bonded continuous sensors described above were used to monitor acoustic emission signals emanating from crack growth in aluminum 7075-T6 and 2024-T3 specimens. It was possible to differentiate the signals due to crack growth from noise signals arising from fretting and RF pickup. The sensitivity of the bonded continuous sensor was comparable to commercial high sensitivity resonant frequency AE sensors. The relationship between acoustic emission parameters and the crack growth rate in the aluminum specimens is examined.

15. SUBJECT TERMS
Structural health monitoring, acoustic emission, crack growth rate, acoustic emission energy, continuous sensors

16. SECURITY CLASSIFICATION OF:			17. LIMITATION OF ABSTRACT:	18. NUMBER OF PAGES	19a. NAME OF RESPONSIBLE PERSON (Monitor)
a. REPORT	b. ABSTRACT	c. THIS PAGE			William Freemantle
Unclassified	Unclassified	Unclassified	SAR	36	19b. TELEPHONE NUMBER *(Include Area Code)* N/A

Standard Form 298 (Rev. 8-98)
Prescribed by ANSI Std. Z39-18

PREPRINT

TABLE OF CONTENT

ABSTRACT

Fatigue crack growth during the service of aging aircrafts has become an important issue and the monitoring of such cracks in hot spots is desirable. A structural health monitoring sensor system that uses acoustic emission technique for monitoring safety of such structures is described in this report. A “continuous sensor” formed by connecting multiple sensor nodes in series arrangement to form a single channel sensor is proposed to monitor acoustic emission signals. This report describes the work performed for monitoring fatigue cracks in aluminum lap joints. The traditional AE sensors as well as bonded continuous sensors described above were used to monitor acoustic emission signals emanating from crack growth in aluminum 7075-T6 and 2024-T3 specimens. It was possible to differentiate the signals due to crack growth from noise signals arising from fretting and RF pickup. The sensitivity of the bonded continuous sensor was comparable to commercial high sensitivity resonant frequency AE sensors. The relationship between acoustic emission parameters and the crack growth rate in the aluminum specimens is examined.

KEYWORDS: Structural health monitoring, acoustic emission, crack growth rate, acoustic emission energy, continuous sensors.

1.0 INTRODUCTION

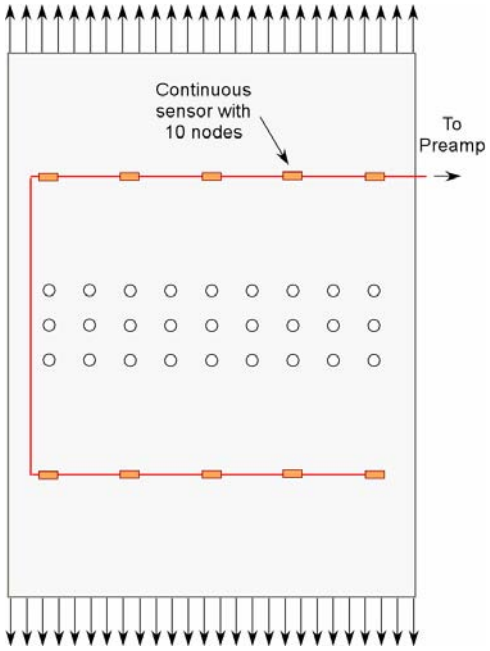

Figure 1. Continuous sensor for monitoring multiple damage sites.

The structural integrity of aging aircrafts has become an important concern. In particular regions around stress risers such as riveted joints and bolt holes are potential sources of fatigue cracks. Continuous monitoring of such hot spots during service is desirable. Acoustic emission (AE) technique has the potential to detect very small rates of crack growth while the structure is in service. There are however some important limitations for the conventional acoustic emission technique, which include the susceptibility to a variety of noise sources, inability to quantify the damage, and the need for an extensive network of sensors and instrumentation. Some of these limitations can be overcome by a new sensor and instrumentation recently proposed [1]. Figure 1 shows schematic illustration of a continuous sensor for monitoring multiple damage sites using a single channel “continuous sensor”. The continuous sensor is formed by connecting a number of individual bonded AE sensors in electrical series connection [2] and is shown to retain the sensitivity of a comparable single node AE sensor. In the present situation a single channel continuous sensor would be able to monitor

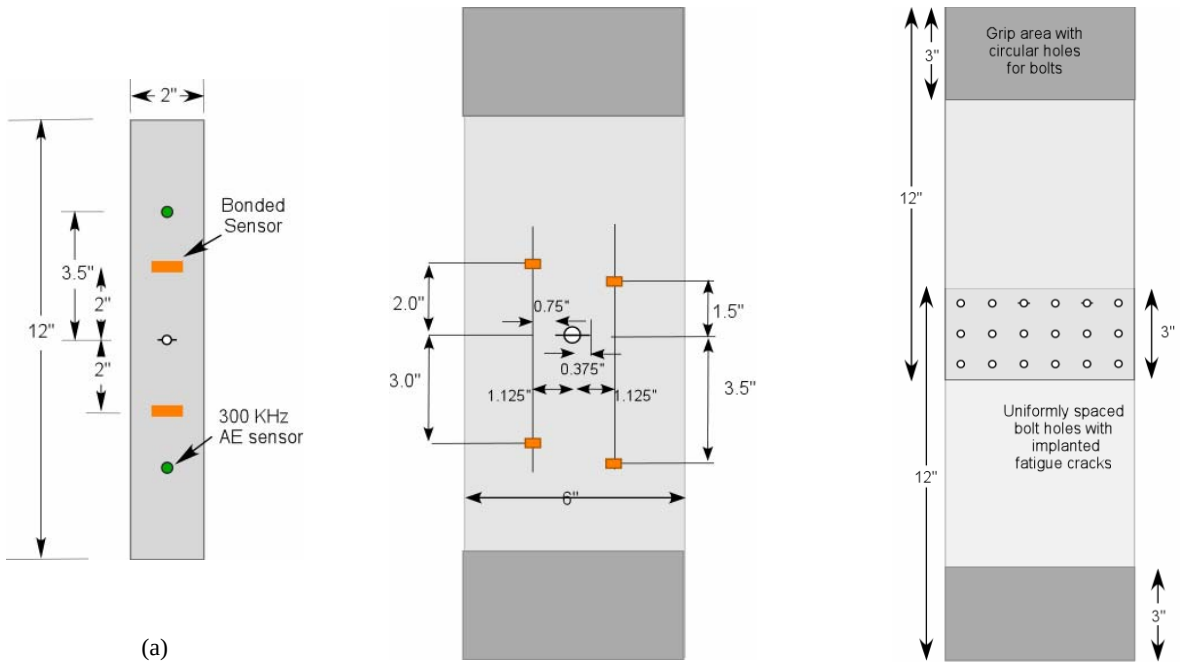

(a) (b) (c)

Figure 2. Specimens used for monitoring fatigue crack growth in 7075-T6 Aluminum: (a) 2-inch wide coupon with central crack, (b) 6-inch coupon with central crack; and (c) 6 inch wide lap joint with a crack near a bolt hole. The thickness of all the specimens was 0.125 inches.

fatigue crack growth from multiple holes in the specimen shown in Figure 1. In this case, since the source to sensor distances for the potential crack growth sites are reasonably small, it is expected that the sensitivity of such a system would be high. A structural health monitoring system based on the continuous sensor is described in reference 6. The objective of the present work was originally set to monitor fatigue crack growth in 7075-T6 lap joints using continuous sensors. Subsequently it was suggested that 2024-T3 aluminum lap joints be monitored for fatigue cracks around rivet holes. The AE signals from fatigue crack growth in aluminum typically are of very small amplitude. This small amplitude combined with the presence of various sources of noise signals present in the environment pose unique challenge in the structural health monitoring application. However, if these problems are overcome, the acoustic emission technique has the ability to quantify the crack growth rate and directly assess the damage criticality in real time.

Acoustic emission technique has been applied to monitor fatigue crack growth in aluminum alloys in several previous investigations. The work of Harris and Tetelman [3] and Harris [4] were two of the earliest studies to relate crack growth in aircraft aluminum alloys with acoustic emission parameters. More recently, Searle et. al. [5], studied the feasibility of detecting crack growth in relatively thick aluminum plates with acoustic emission waveforms. Most studies on acoustic emission in aluminum alloys focus on plates that are thicker than 0.25 inches. Further developments in the use of continuous sensor for structural health monitoring are described in reference 6.

2.0 SPECIMEN DESCRIPTION

Three different specimen configurations shown in Figure 2 were fabricated to determine the feasibility of detecting fatigue crack growth in aluminum lap joints. Two types of materials were used for these specimens. The first group of specimens were fabricated from 0.125” thick 7075-T6 sheets and the second group of specimens were fabricated from 1mm thick 2024-T3 sheets. The first specimen was 2 inch wide and either 12 or 18 inch long, with a 0.125-inch circular

Figure 3. Part of the total number of specimens that were fabricated, precracked, and tested for developing the structural health monitoring technique.

hole in the middle. Horizontal saw cuts were made on either side of the circular hole and fatigue pre-cracks were initiated from these notches through cyclic loading. Once measurable crack lengths were seen, these specimens were further subjected to fatigue loading and the acoustic emission signals from the cracks were continuously monitored. The second specimen was 6 inch wide and 16 inch long with a 0.25-inch diameter hole at the center and similar precracks. The third specimen was a riveted lap joint specimen in which a pre-crack was initiated at one of the rivet holes. In addition, three lap joint specimens from an aircraft fuselage were supplied by the AFRL ML. Two of these specimens were instrumented with sensors. One of these specimens was fatigue tested to failure.

3.0 INSTRUMENTATION

Commercial 150 kHz as well as 300 kHz resonant frequency sensors were used for evaluating the performance of the bonded continuous sensors used in this study. The bonded sensors were made of PZT-5A wafers with top and bottom electrodes connected in a series configuration. An epoxy layer was initially placed on the aluminum plates to provide electrical shielding for the sensing element. Coupon specimens were instrumented with single element bonded sensors as shown in Figure 2. For the 6 inch wide panel and 6 inch wide lap joints continuous sensors with either two or three nodes connected in series were used. For most of the tests reported here commercially available 50 kHz to 5 MHz wide band voltage amplifier was employed for amplification of the signals from the sensors. The amplified signals were acquired using a digital oscilloscope typically at 10^7 samples per second. The performance of the bonded sensor nodes and the commercially available sensors were compared using both simulated AE signals as well as actual AE signals collected during fatigue crack growth under cyclic loading. The digitized signals were further filtered to eliminate noise outside the band of 100 kHz and 700 kHz. This low frequency component can be removed either through appropriate front-end filters or through digital filtering. All the specimens except the last specimen described above were tested

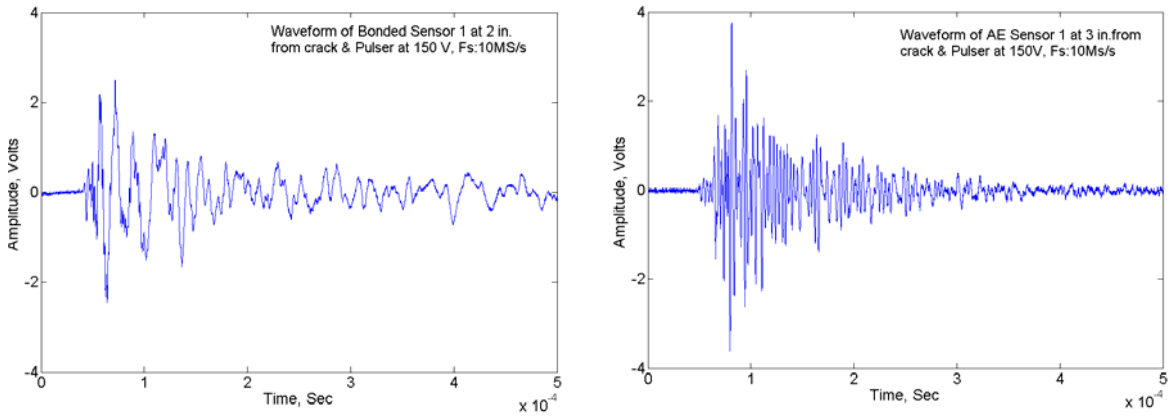

(a) (b)

Figure 4. Signals corresponding to the simulated acoustic emission signals: (a) Bonded AE sensor, (b) Commercial 300 kHz resonant frequency sensor

using the wide band voltage amplifier and the data was acquired using digital oscilloscope. The noise outside the desired frequency band was removed using digital filter for all specimens except for the last specimen. The KC-135 fuselage panel was tested using the NI 6115 data acquisition board and the amplifier provided by Triad Semiconductor, which had front-end analog as well as digital filters. The results shown here used digital filtering to eliminate the low frequency components in the bonded sensor signal.

The specimens were cyclically loaded in a 20 kip MTS testing machine. Suitable grips were fabricated for loading the specimens under tension-tension loading. The crack growth rates reported in these experiments were initially measured through a low powered hand held magnifier. Later, a traveling microscope with a magnification of 45x and a micrometer for accurate measurement of the crack length were used.

4.0 COMPARISON OF SENSITIVITY OF THE BONDED CONTINUOUS SENSOR WITH COMMERCIAL AE SENSORS

The sensitivity of the bonded sensor that was used in this study was evaluated through simulated acoustic emission events. Stress waves were launched into the plate through a 0.0625 aperture pulsing transducer that was pulsed with a 150V 50 ns pulse. The resulting stress waves were sensed by the bonded continuous sensor as well as commercially available 300 kHz resonant frequency sensors. For both the 2-inch wide coupon as well as the 6-inch wide specimen this pulsing transducer was located near the central fatigue crack and the signals from both the bonded sensor as well as the 300 kHz resonant frequency sensors were recorded. Figure 4 compares the signal obtained by a single node bonded sensor with that obtained by a 300 kHz AE sensor. The signal amplitude of the bonded sensor is comparable to the high sensitivity commercial sensor. In addition, the bonded sensor exhibits wide band characteristics while the commercial sensor appears to oscillate at one frequency. Similar results were also obtained from the 6-inch wide panel.

5.0 RESULTS FROM 2 INCH WIDE COUPONS

Figure 5(a) shows a sequence of about 50 acoustic emission events sensed by two 150 kHz resonant frequency sensors attached to a two-inch coupon, during fatigue crack propagation. In Figure 5(b) one of the individual events is shown. The source of each of these signals could be determined from the time difference in the AE signals sensed by the two sensors. In one of these specimens, the average crack growth rates and the average acoustic emission energy per cycle were measured.

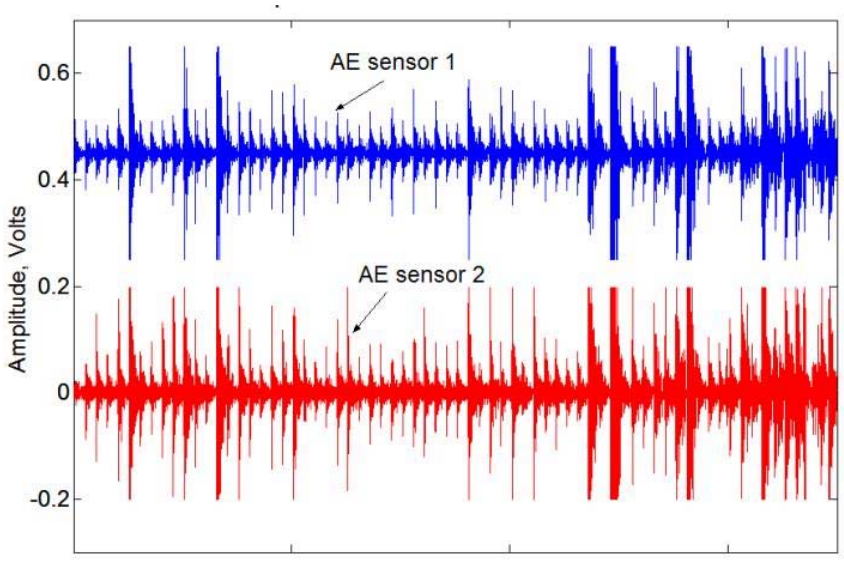

(a)

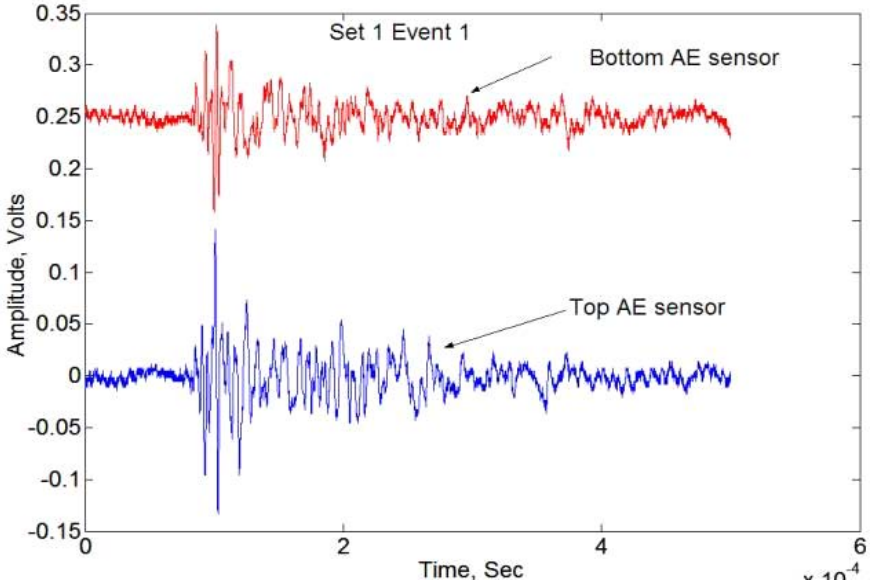

(b)

Figure 5. Acoustic emission signals from fatigue crack in 2-inch wide coupon specimen. (a) Sequence of 50 AE events, and (b) One of the events in the sequence

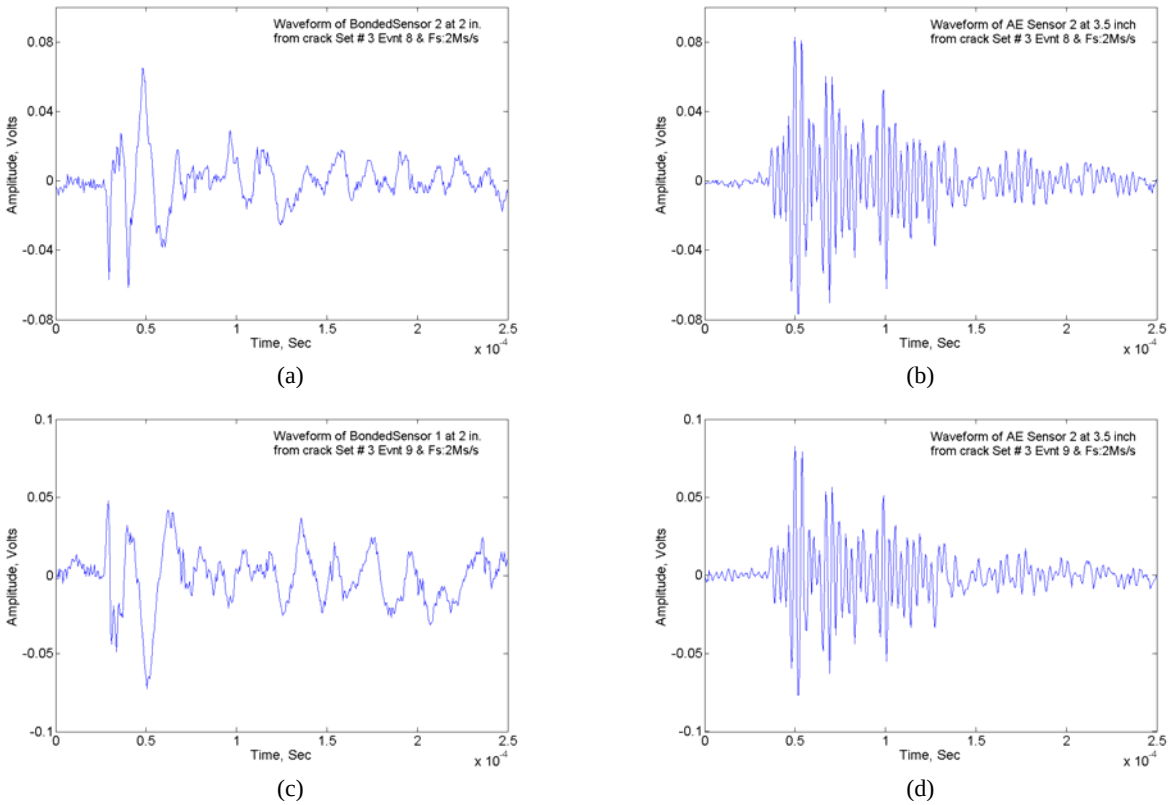

Figure 6. Comparison of AE waveforms from fatigue crack growth in 2 inch wide coupon: (a) and (c) Bonded sensor signals; (b) and (d) 300 kHz commercial AE sensor.

Acoustic emission signals corresponding to crack growth in 2-inch wide specimens

The AE waveforms from the two types of sensors are shown in Figure 6. The amplitude sensitivities of the two sensors are comparable. As in the case of simulated AE signals, the bonded sensor exhibits wide band characteristics. The leading edge of the bonded sensor output has high frequency content while lower frequency components arrive later.

Discrimination between AE signals from fatigue crack growth and noise signals

As mentioned earlier, the susceptibility of the AE technology to various types of noise signals is of great concern. In the current study two types of noise signals were present. The first one is the RF noise due to various sources. In general, it is possible to identify the RF noise from the frequency content, which is generally far above the typical AE signals which are in the frequency band of 100 kHz to 500 kHz and can be eliminated through suitable low pass filtering. The second type of noise is the fretting noise generated through friction between two surfaces moving relative to one another. In the present tests, such noise signals are generated at the grips in the coupon specimens and the lap area in the case of lap joints. The crack growth related AE signals sensed by the bonded sensor have distinctive high frequency components at the leading edge as shown in the top trace of Figure 7(a). Fretting related noise signals do not have such high frequency leading edge and hence can be eliminated if wide band sensors are used. However, the conventional high sensitivity commercial sensor, Figure 7(b), is not able to distinguish between AE signals generated by fatigue crack growth and the fretting related noise because of the resonant frequency response of these sensors.

Relationship between acoustic emission energy and fatigue crack growth

The objective of acoustic emission monitoring is to estimate the rate of crack growth per cycle directly from the AE signals. For 2-inch wide coupon as well as the 6-inch wide panel specimen, the fatigue crack growth rates were measured initially using low power hand held magnifiers at intervals of several thousands of cycles and the average crack growth per cycle was determined. From the AE data collected during such intervals the average acoustic emission energy per cycle was also calculated. Figure 8 shows the variation of the acoustic emission energy per cycle measured

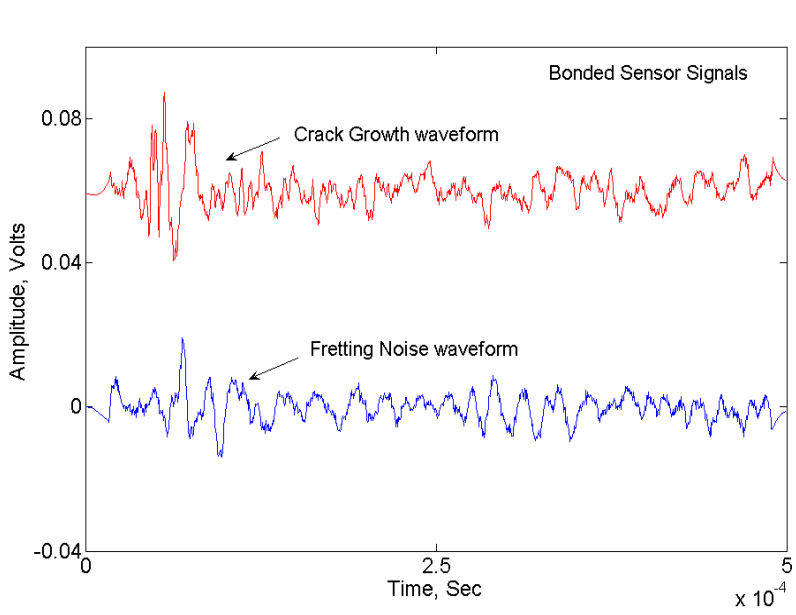

(a)

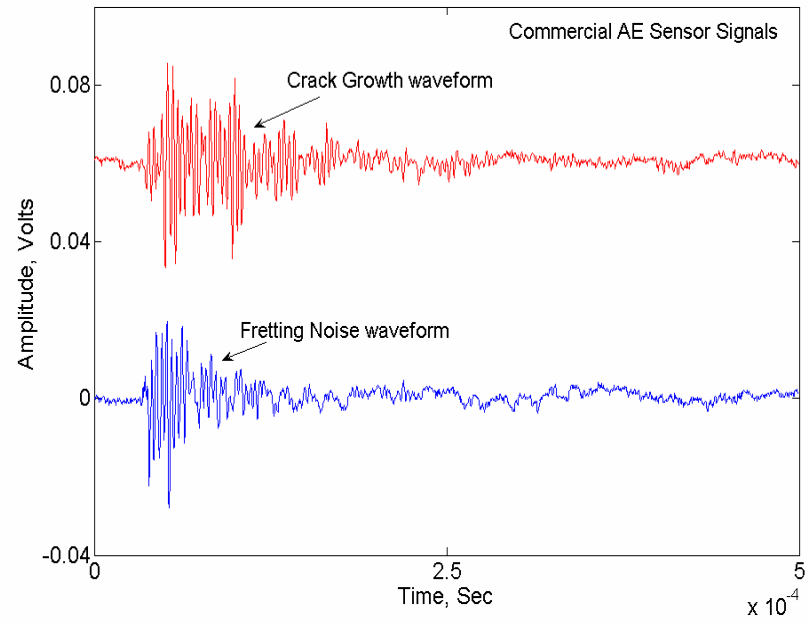

(b)

Figure 7. Comparison of AE waveforms related to crack growth and fretting related noise from the two types of sensors (a) Bonded sensor, and (b) 300 kHz commercial sensor.

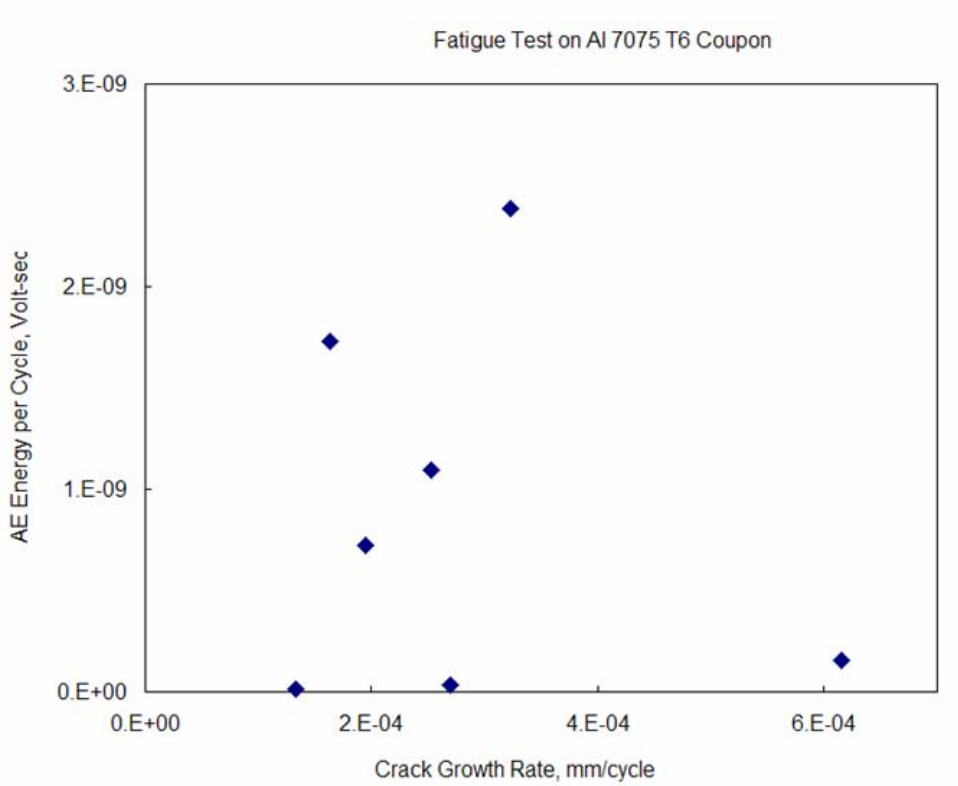

Figure 8. Acoustic emission energy per cycle as a function of fatigue crack growth rate for 2-inch wide coupon specimen.

by the bonded sensor with the fatigue crack growth rate. Lack of good correlation for this plot could be attributed to poor resolution of the hand held magnifier for crack length measurement and the presence of some noise in the signals.

6.0 RESULTS FROM 6 INCH PANEL 7075-T6

The 7075-T6 panel was instrumented with one continuous sensor 2.5 inches above the crack and another continuous sensor 1.5 inches below the crack. Both of these continuous sensors had two nodes each. 300kHz resonant frequency sensors were located at 2 inches above and below the crack. The response of the bonded continuous sensor and resonant frequency sensors corresponding to a simulated AE event are compared in Figure 9. The panel was loaded at a frequency of 5 Hz and the data reported were collected using the wide band preamplifier and oscilloscope mentioned earlier. The cycling was stopped periodically to measure the crack length using a 45X traveling microscope. The crack growth was monitored from an initial length of about 0.375 inch to a final length of nearly 3 inches. A set of waveforms from the two continuous sensors and the two resonant frequency sensors are shown in Figure 10. The waveforms from the continuous sensor contained high amplitude, low frequency components below 100 kHz. These waveforms for the continuous sensor were filtered with a 70 kHz to 500 kHz band pass filter before plotting in these figures. The origin of the signals could be ascertained from the time difference between the top and bottom sensor signals. Hence, it was possible to determine if the signals were from the fatigue crack at the center of the panel or from the fretting in the grip area. Two events whose sources were identified are plotted in Figure 13. The signals in the bottom row were from the bonded continuous sensor. The signal due to fatigue crack growth generally had short rise time and higher frequency content in the beginning, while the fretting related signals had longer rise time and smaller amplitude. However, it was not possible to discriminate between the crack growth related signals and fretting related signals from the resonant frequency sensor. For this panel almost all the signals recorded were from fatigue crack growth. The energy content in these waveforms was calculated and from the total energy recorded during the periodic stops of cycling, the AE energy per cycle was determined. Figure 14 shows the plot of the AE energy per cycle vs. the crack growth rate da/dN.

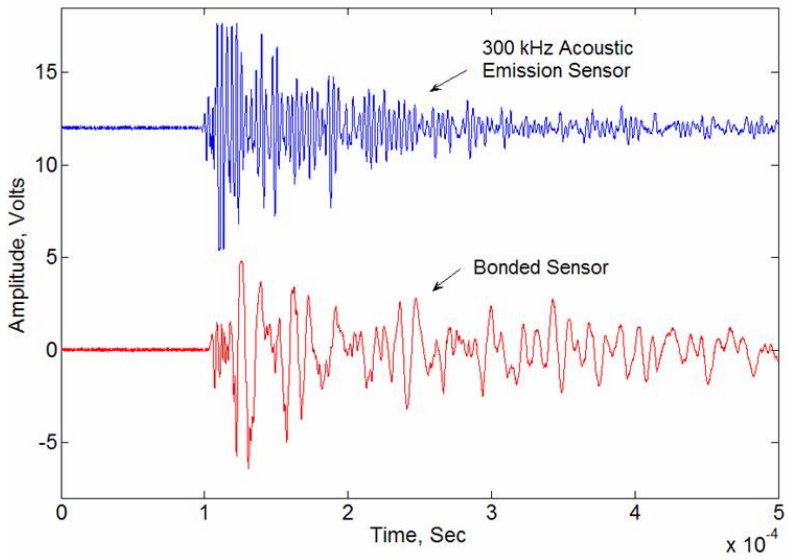

Figure 9. Simulated acoustic emission event showing comparison of responses of the resonant frequency sensor and the bonded continuous sensor

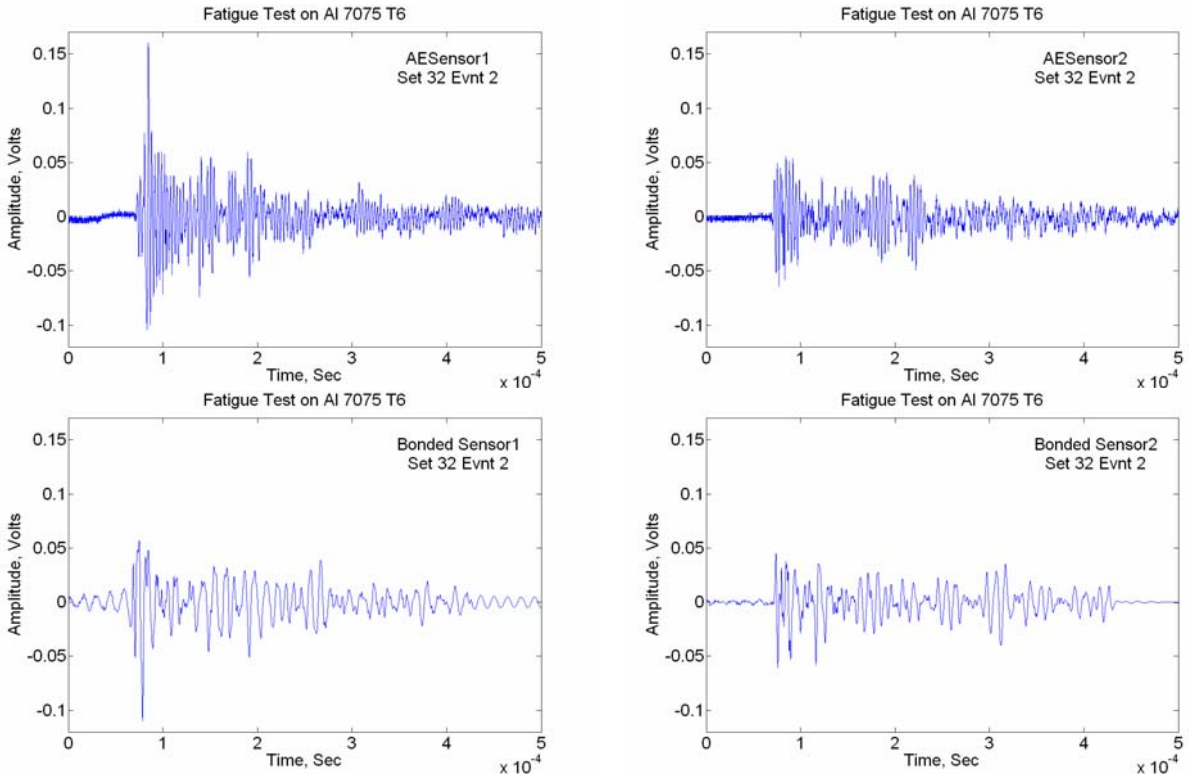

Figure 10. Waveforms corresponding to a crack growth event in 0.125” thick 7075-T6 panel with central crack

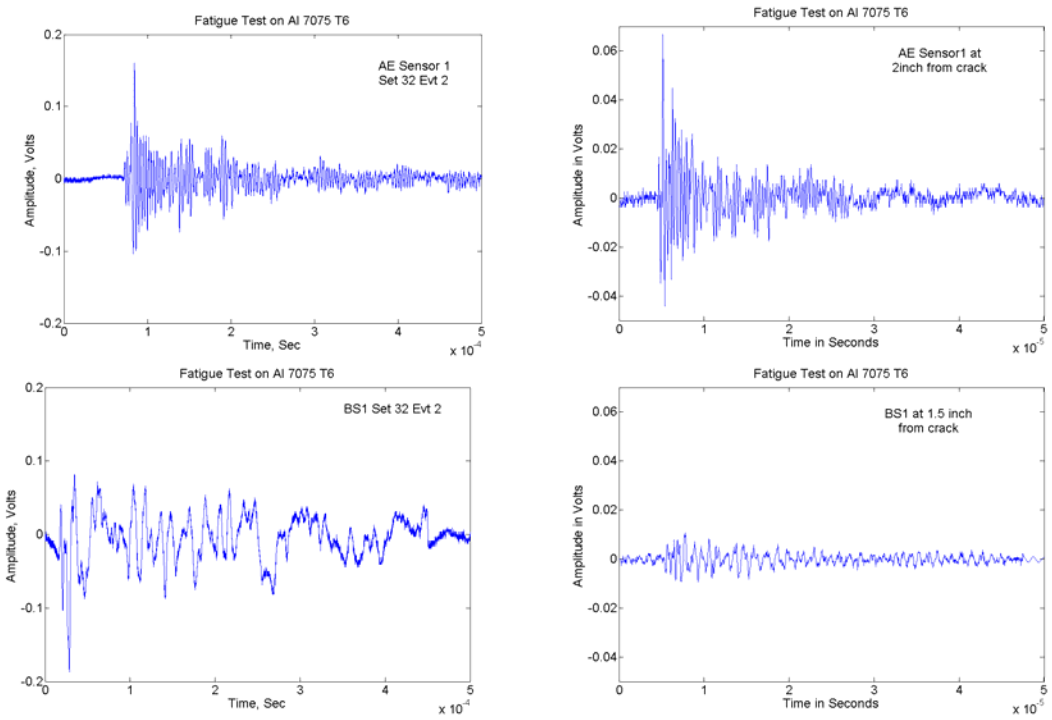

Figure 11. Waveforms corresponding to crack growth related events (left) and fretting related event (right) from the two types of sensors. The waveforms shown in the top are from 300 kHz resonant frequency sensors and those below are due to the bonded continuous sensor.

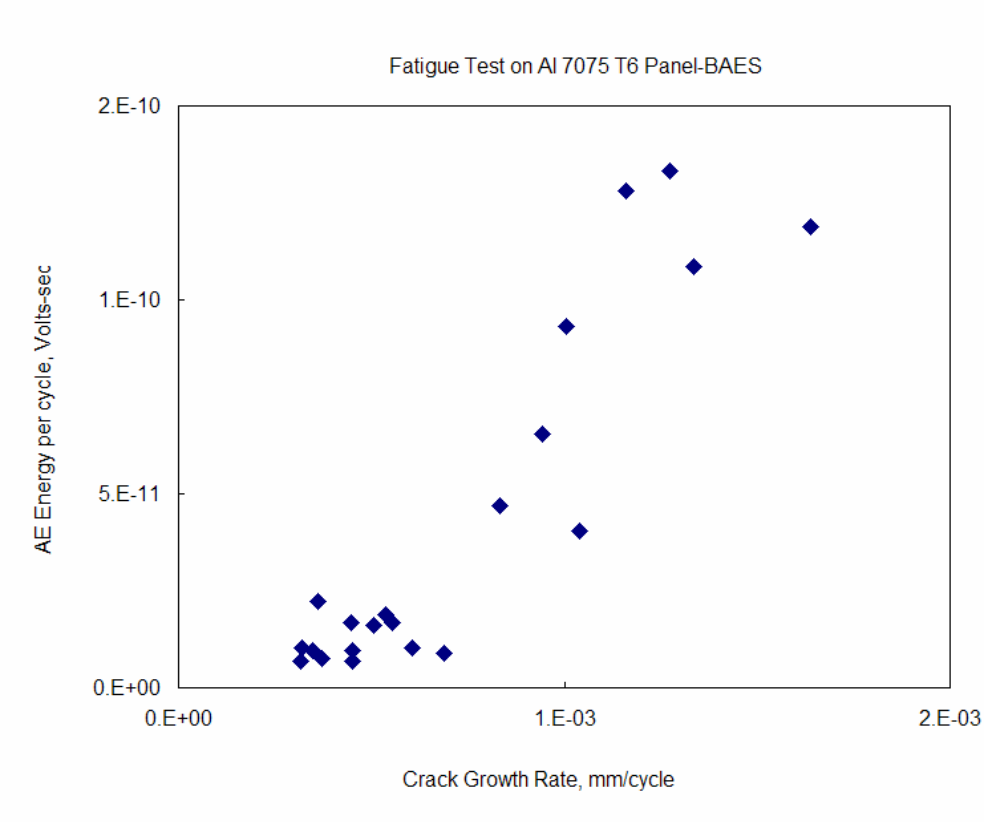

Figure 12. Relationship between the crack growth rate and the acoustic emission energy per cycle for 0.125 inch thick 7075-T6 panel.

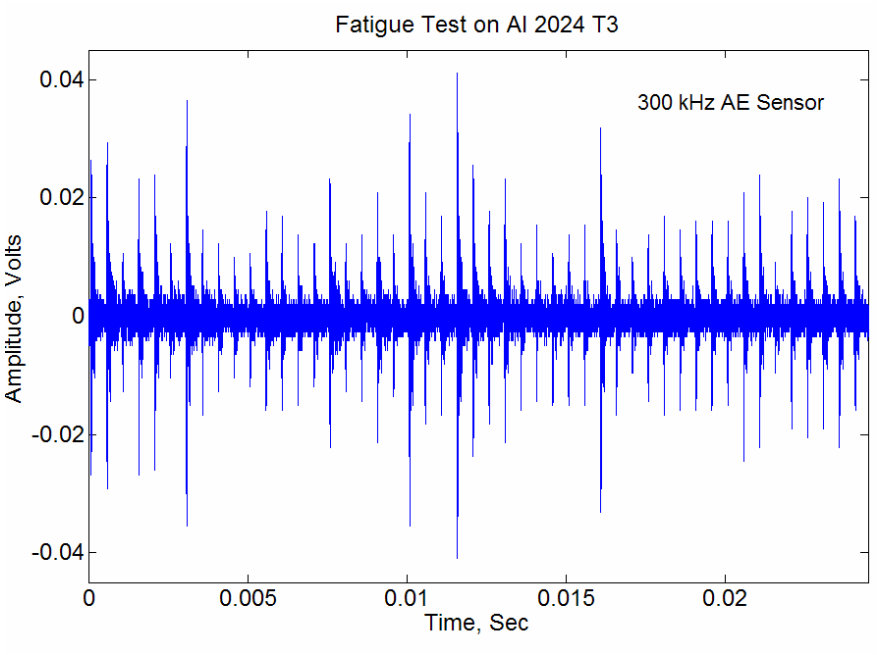

(a)

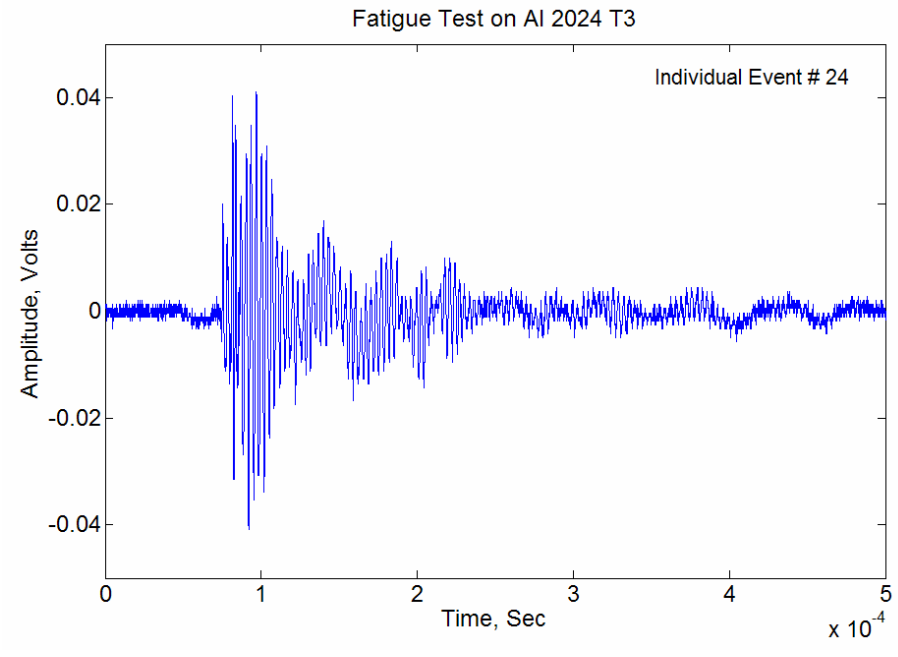

(b)

Figure 13. AE Signals from 300 kHz resonant frequency sensor due to fatigue crack growth in 2024-T3Aluminum Panel; (a) Sequence of 49 AE events, and (b) One of the events in the sequence

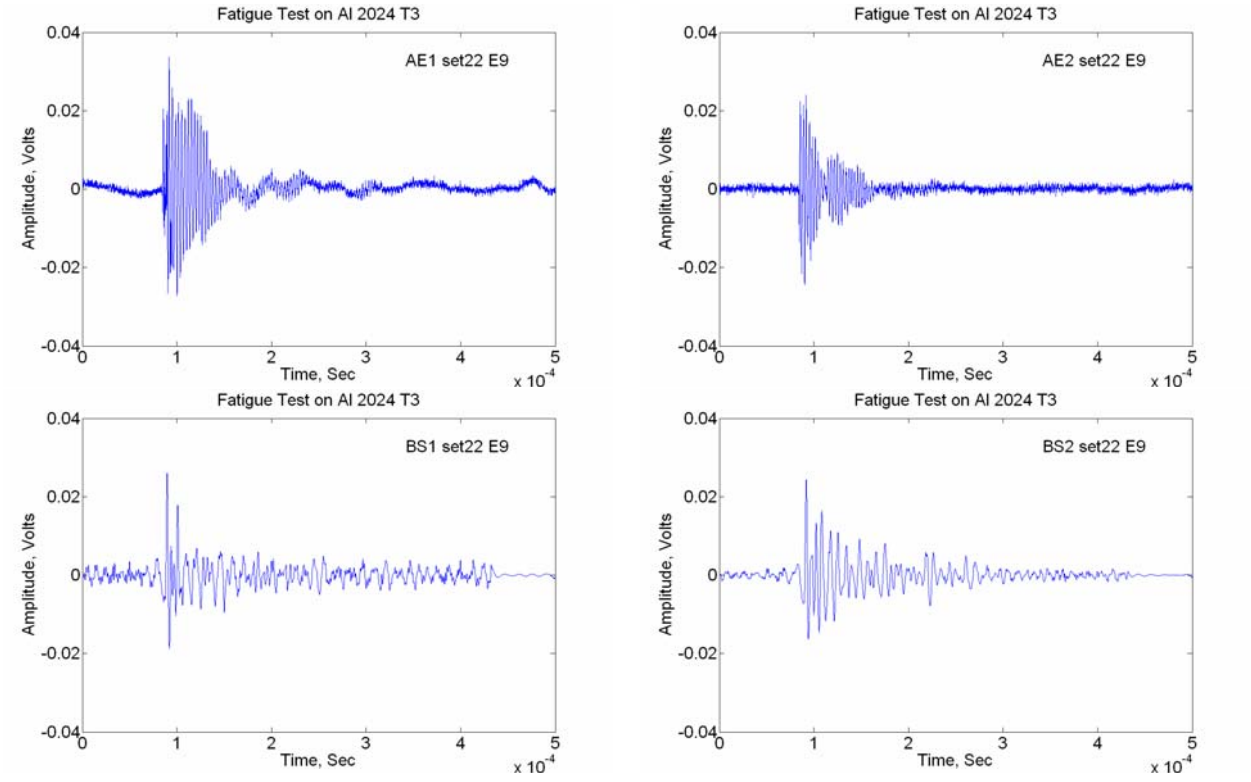

Figure 14. Waveforms corresponding to crack growth related event. The waveforms shown in the top are from 300 kHz resonant frequency sensors located above and below the central crack and the waveforms shown in the bottom are those due the corresponding bonded continuous sensors.

7.0 RESULTS FROM 2024-T3 PANEL

A 2024-T3 panel was initially instrumented with two 300 kHz resonant frequency sensor to observe the fatigue crack growth related AE signals, this panel was cyclically loaded to grow the fatigue crack by about 0.25 inch. One sequence of AE signals from the fatigue crack growth is shown in Figure 13. Subsequently this panel was instrumented with continuous sensor and the fatigue crack growth was monitored. The acoustic emission signals from the 1 mm thick 2024-T3 panels shown in Figure 14 were smaller in amplitude compared to those observed in 7075-T6 panel. The plot of the AE energy per cycle vs. crack growth rate da/dN is shown in Figure 15.

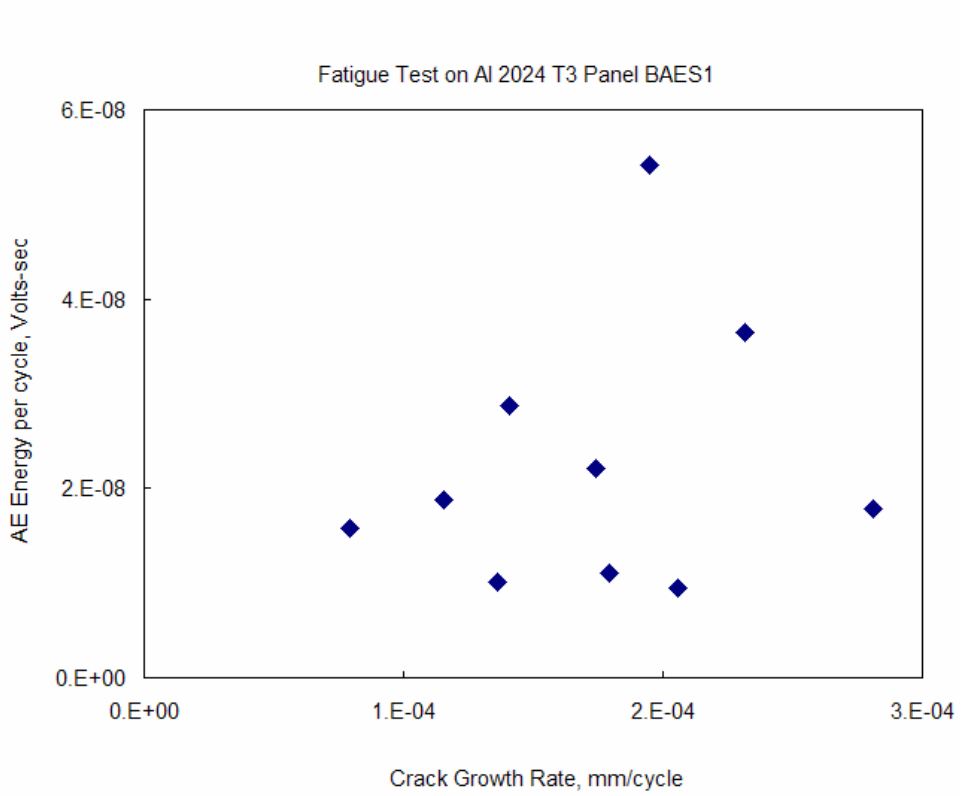

Figure 15. Plot of AE energy/cycle versus crack growth rate for 2024-T3 panel.

8.0 MONITORING LAP JOINT SPECIMENS

The 7075-T6 lap joint was fabricated from a 1 mm thick plate. The specimen was fabricated with a pre-crack at the central bolt hole in the bottom row of the lower plate. It was instrumented with two continuous sensors with 3 nodes each, one in the top plate of the joint and the other in the bottom plate. In addition, two 300 kHz resonant frequency sensors were also located nearly at the same distance as the bonded continuous sensors in the two plates. The specimen was cycled at 1 to 3 Hz loading rate and acoustic emission waveforms were recorded using wideband voltage amplifier and digital oscilloscope. Representative waveforms from the crack growth are shown in Figure 16.

The next set of waveforms is from the 2024-T3 lap joint that was fabricated from a 1 mm thick plate. The specimen was fabricated with a pre-crack at the central bolt hole in the bottom row of the lower plate. It was instrumented with two continuous sensors with 3 nodes each, one in the top plate of the joint and the other in the bottom plate. In addition, two 300 kHz resonant frequency sensors were also located at equidistance from the crack on the bottom plate. This specimen was also cycled at 1 to 3 Hz loading rate and acoustic emission waveforms were recorded using wideband voltage amplifier and digital oscilloscope. Representative waveforms from the crack growth are shown in Figure 17.

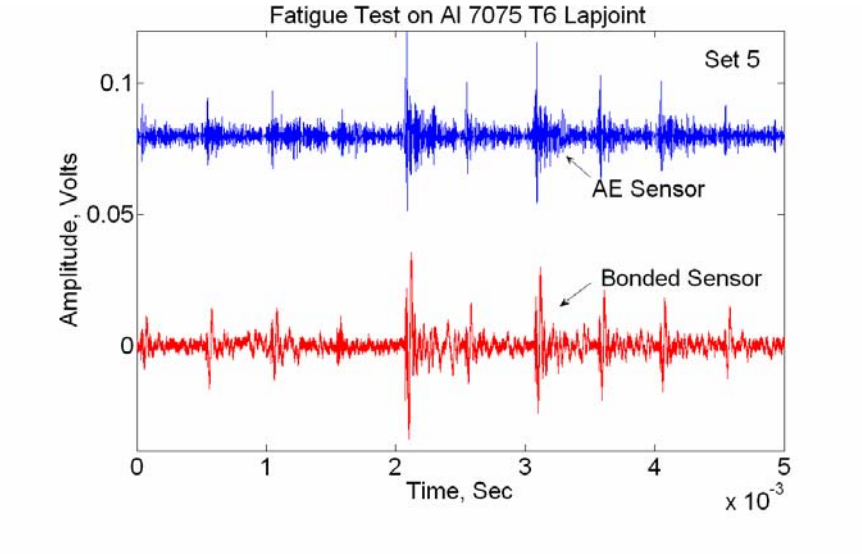

(a)

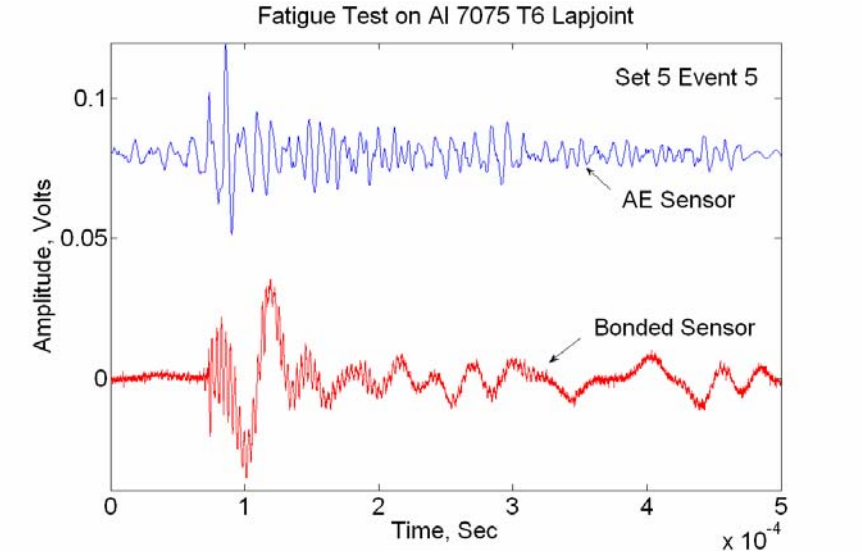

(b)

Figure 16. Acoustic emission signals recorded from the 7075-T6 lap joint; (a) a sequence of events recorded during the fatigue loading; (b) an event from this sequence magnified along the time axis.

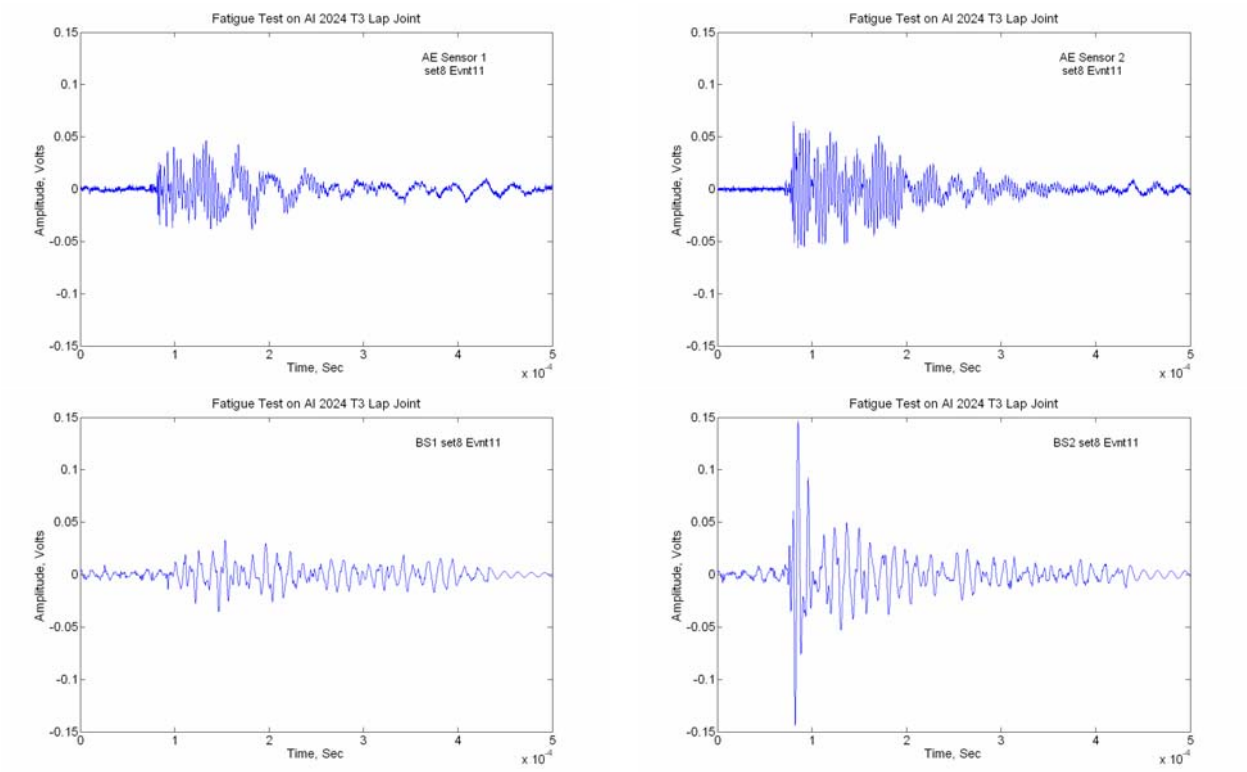

Figure 17. Acoustic emission waveforms from crack growth in 2024-T3 aluminum lap joint. The top two traces are from 300 kHz resonant frequency sensors located above and below the fatigue crack, on the cracked half of the lap joint. The bottom right waveform is from the continuous sensor on the cracked half of the lap joint and the bottom right waveform is from the un-cracked half of the lap joint.

9.0 MONITORING CRACK GROWTH IN A LAP JOINT FROM KC-135 FUSELAGE

Two lap joint specimens extracted from the KC-135 fuselage were 6 inches wide and about 20 inches long. They were gripped using steel doubler plates bolted across the edges and loaded in a 5000 lbs capacity MTS testing machine at University of Dayton Research Institute facility. These specimens were instrumented with two continuous sensors located 1.5 inches above and below the lap area. Each of these continuous sensors had three nodes equally spaced along the specimen width. The bonded continuous sensors were tested using simulated acoustic emission signals from a pulser and were found to have sensitivity comparable to the 300 kHz resonant frequency sensors. Results from testing one of these lap joints is described under this section. The panel with the continuous sensor is shown in Figure 18. Test was performed over three days, sequentially increasing the load. The fatigue loading on this panel was gradually increased until the specimen failed. The seven sequences and the corresponding minimum and maximum loads are shown in Figure 19. The regions between successive pairs of markers represent a sequence. The final load amplitude was between a minimum load of 150 lbs and maximum load of 4450 lbs. The lap joint failed at about 357,000 cycles in the grip area. There was gradually increasing separation of the two halves of the lap joint during later stages of the fatigue loading and the sealant in this area was disintegrating and was squeezed out. The instrumentation consisted of Triad Semiconductor's charge amplifier and the PXI 6115 board. The data acquisition was performed using the LabView software. The threshold level for recording the signal was adjusted during each phase to ensure that excessive numbers of AE events were not collected and focus of the study was mainly on the relatively high amplitude events during each segment of the fatigue loading.

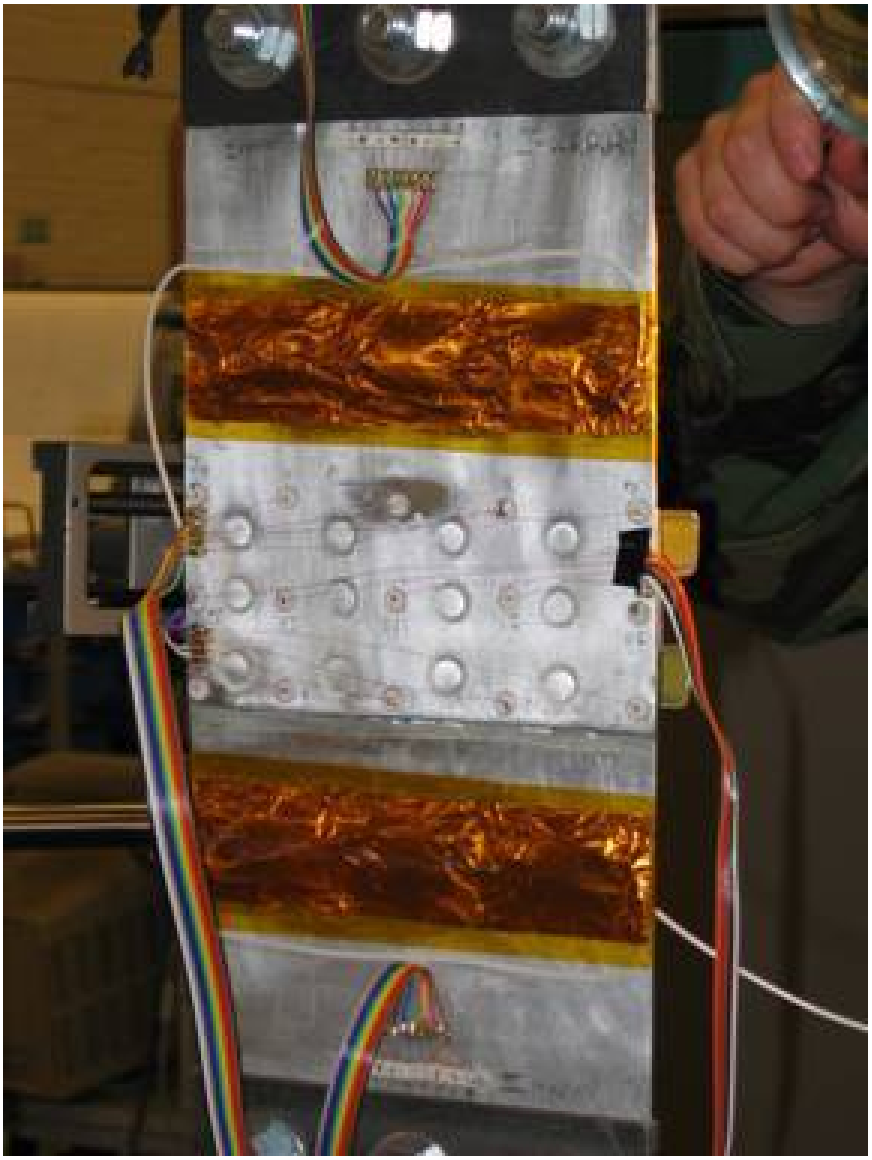

Figure 18. Lap joint extracted from KC-135 fuselage section with the two continuous sensors.

The gain of the charge amplifier in the beginning of the experiments was estimated to be 1600 or 64 dB. During the 5th segment of loading some of the AE signals were exceeding 20V p-p and hence were saturating the amplifier and reduction in gain was needed to properly quantify the highest amplitude signals generated towards the end of the test. The new gain was estimated to be 400 or 52 dB. The amplitudes of the acoustic emission events shown in table 1 were adjusted to reflect an effective gain of 400x or 52dB.

During the initial five segments of loading the typical acoustic emission amplitudes were relatively small and were in the range of 2 to 3 V. There were a few events with amplitude of 5V. These amplitudes increased to 3 to 5V during the 6th segment. Very few 20 V p-p events were also seen. During the 7th and final segment during which the specimen failed, the typical AE event amplitude increased to 8 to 15V. Significant number of events (about 10%) was exceeding the amplifier limits of 20V p-p even at the reduced gain of 52 dB. Some characteristics of the AE events during each of the segments of fatigue loading are shown in table 1. In the beginning most of the events had longer rise time and longer duration. These events are likely to be from fretting in the grip or lap area. Towards the end of the test larger proportion of events had short rise time and short duration. These events are likely to be from fatigue cracks. Three of the sequences

each containing 50 events each collected during a small number of cycles at various stages of the fatigue loading are described here. The first of these sequences, recorded during the 2nd segment of fatigue loading is shown in Figure 20. A series of 50 events shown in the top of this Figure and the single event from this sequence that is magnified along the time axis shown in the bottom of the Figure. It may be observed that most of these events have relatively large rise time (larger than 15 microseconds) and large duration (above 300 microseconds). The second sequence shown in Figure 21 was recorded during the seventh segment of fatigue load during which the cyclic amplitude was the highest. However, during a short period of this segment, the cyclic frequency was increased from 10 Hz to 20 Hz. This increase in the frequency of fatigue load resulted in excessive vibration of the specimen and hence, the frequency was changed back to 10 Hz within a short time. The sequence shown in Figure 21 were recorded during this period when the cyclic frequency was at 20 Hz, and most of the signals during this period are believed to be due to fretting caused by the excessive vibration. Relatively long rise time and duration are seen in these events and hence they are similar to the events seen during the second sequence of fatigue load.

The third sequence of events shown in Figure 22 was recorded towards the end of the seventh sequence of fatigue load. These events had predominantly short rise time, less than 7 microseconds and short duration, less than 150 microseconds. Further, most of these signals arrived at the bottom continuous sensor first and later at the top continuous sensor. The amplitude of the signals from the lower continuous sensor was larger than the top continuous sensor. The arrival time difference along with the short rise time and short duration of these events suggest the initiation and propagation of a crack near the bottom row of rivets in the lower half (thick panel) of the riveted joint. This hypothesis has to be confirmed by visual inspection or by other means.

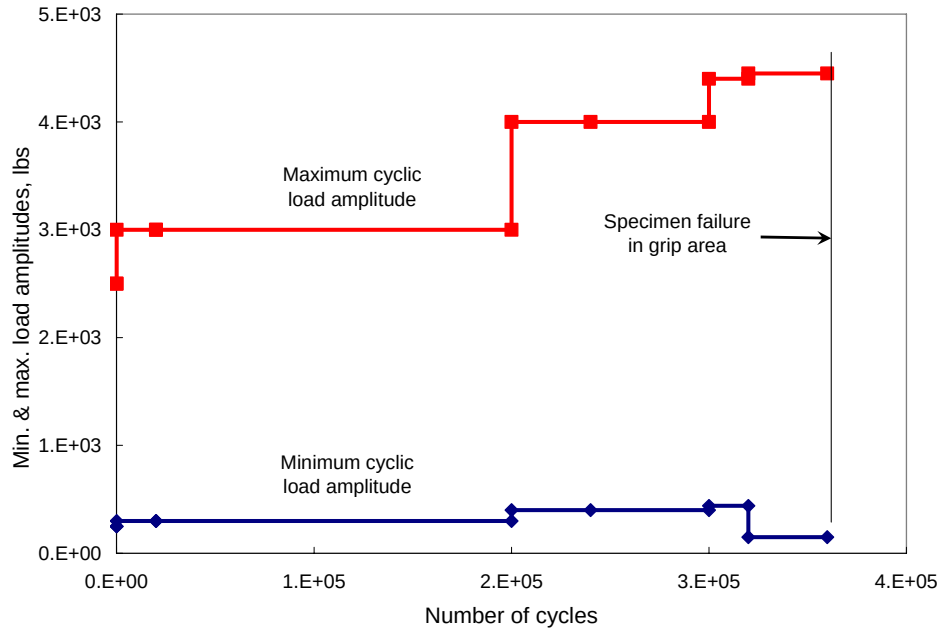

Figure 19. Minimum and maximum load amplitudes applied during the fatigue testing of lap joint from a KC-135 aircraft fuselage.

Table 1. Details of the fatigue load segments and the acoustic emission events collected during these sequences.

Fatigue Loading Segment No.	Estimated No. of Fatigue Cycles	No. of events recorded	Percentage of Short RT events	Typical Amplitudes of Short RT events	Percentage of Long RT events	Typical Amplitudes of Long RT events
1	53	200	<1%	3V	99%	2.5V
2	19,947	1,000	<1%	2.5V	99%	2V
3	40,000	800	4%	2V	96%	2V
4	140,000	7,650	12%	2.5V	88%	3.75V
5	86,621	9,100	13%	2V	87%	2V
6	50,000	14,000	19%	3 to 5V	81%	3 to 6V
7	23,258	2,540	47%	8 to 15V	53%	8 to 12 V

The fourth sequence shown in Figure 23 was recorded very near the failure of the specimen. This sequence of events also had predominantly short rise time and short duration events similar to the events shown in Figure 22. Such events, however, arrived at the top sensor first before reaching the bottom continuous sensor. The amplitude of the signals from the top continuous sensor was larger than the bottom continuous sensor. The arrival time difference along with these signal characteristics suggests the presence of a crack above the top continuous sensor in the thin panel. Since the final failure was caused by crack growth in the top grip area, the signals recorded does correlate with the crack growth in the grip area. This unexpected failure event in the grip region does emphasize the advantage of the acoustic emission technique in that one does not have to know the location of the potential failure location in the region that is being monitored to detect dangerous levels of crack growth rates.

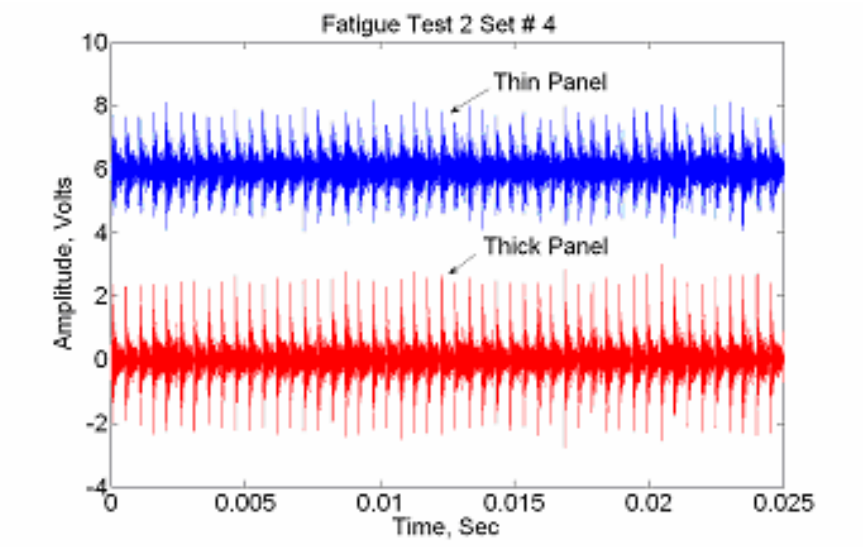

(a)

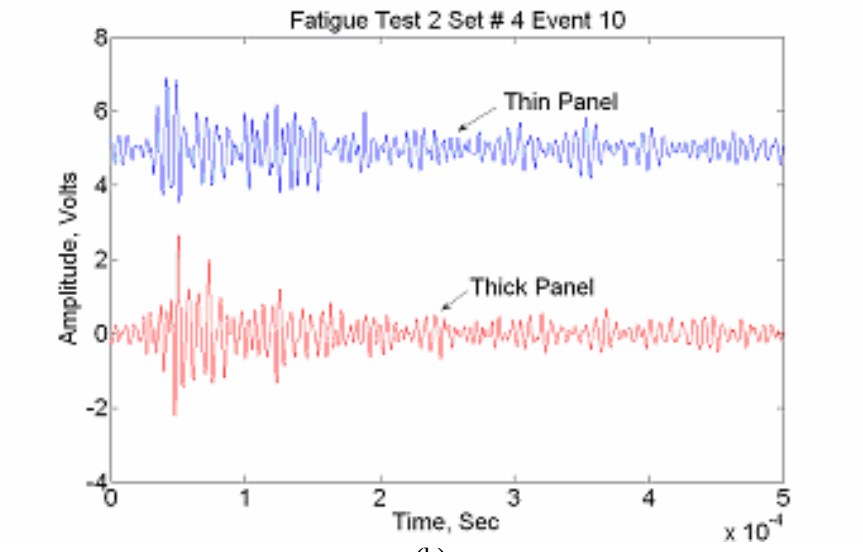

(b)

Figure 20. (a) A sequence of AE events recorded during the second segment of fatigue load and (b) one of these events magnified along the time axis.

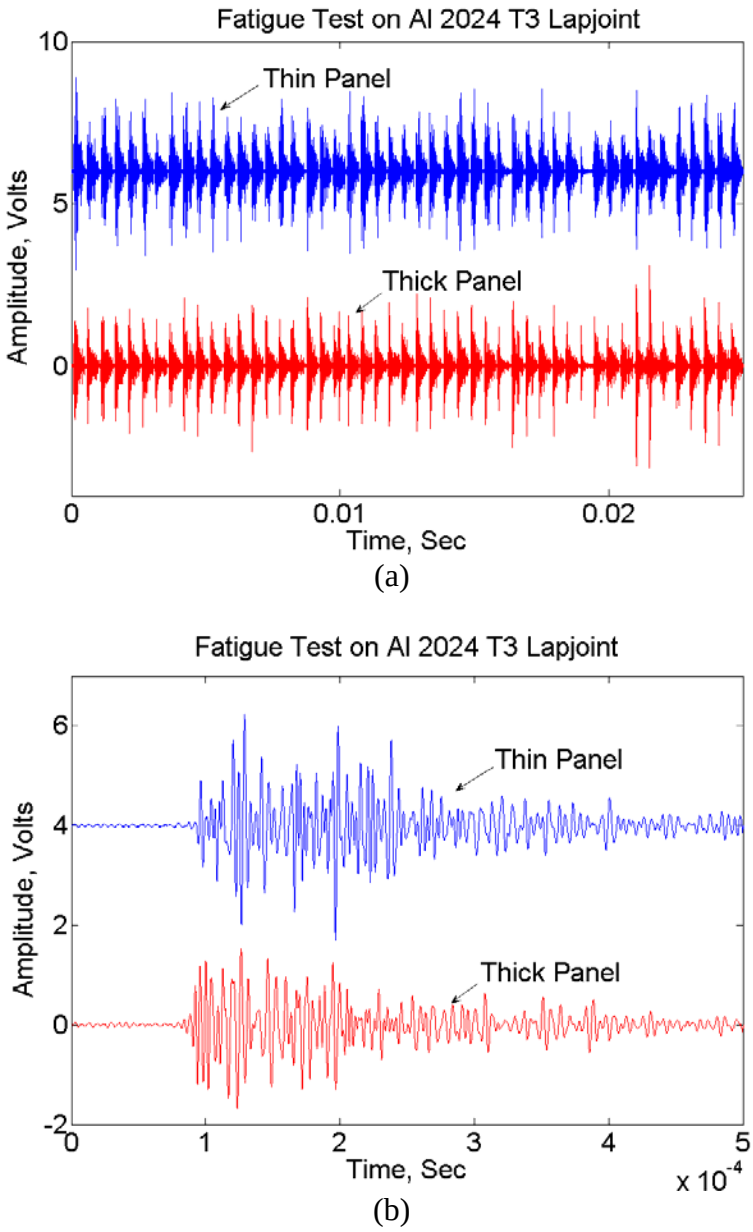

Figure 21. (a) A sequence of AE events recorded during the seventh segment of fatigue load during which the loading frequency was increased to 20 Hz resulting in excessive specimen vibration and (b) one of these events magnified along the time axis.

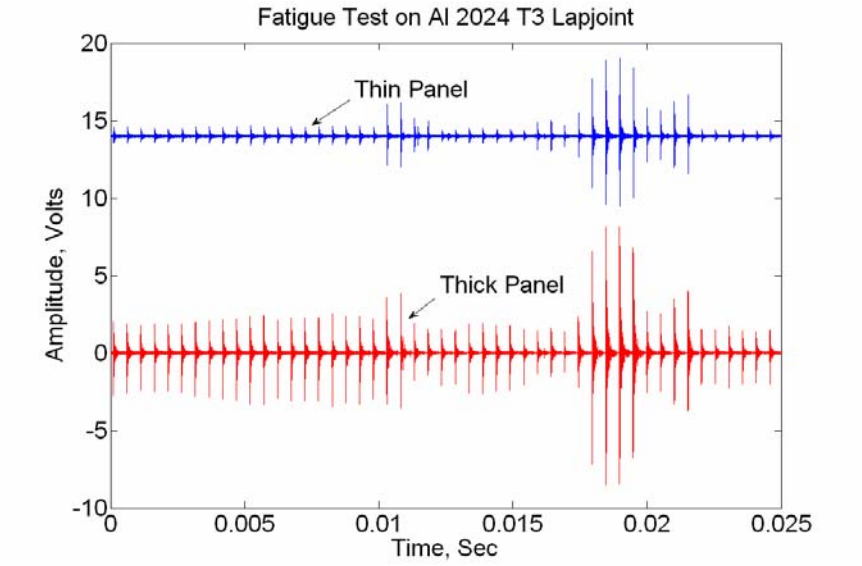

(a)

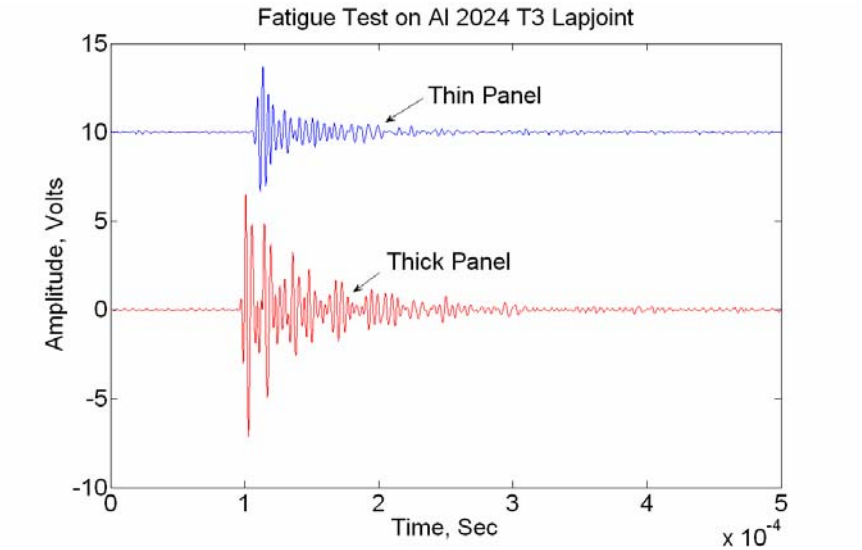

(b)

Figure 22. (a) A sequence of AE events recorded towards the end of the seventh segment of fatigue load and (b) one of these events magnified along the time axis.

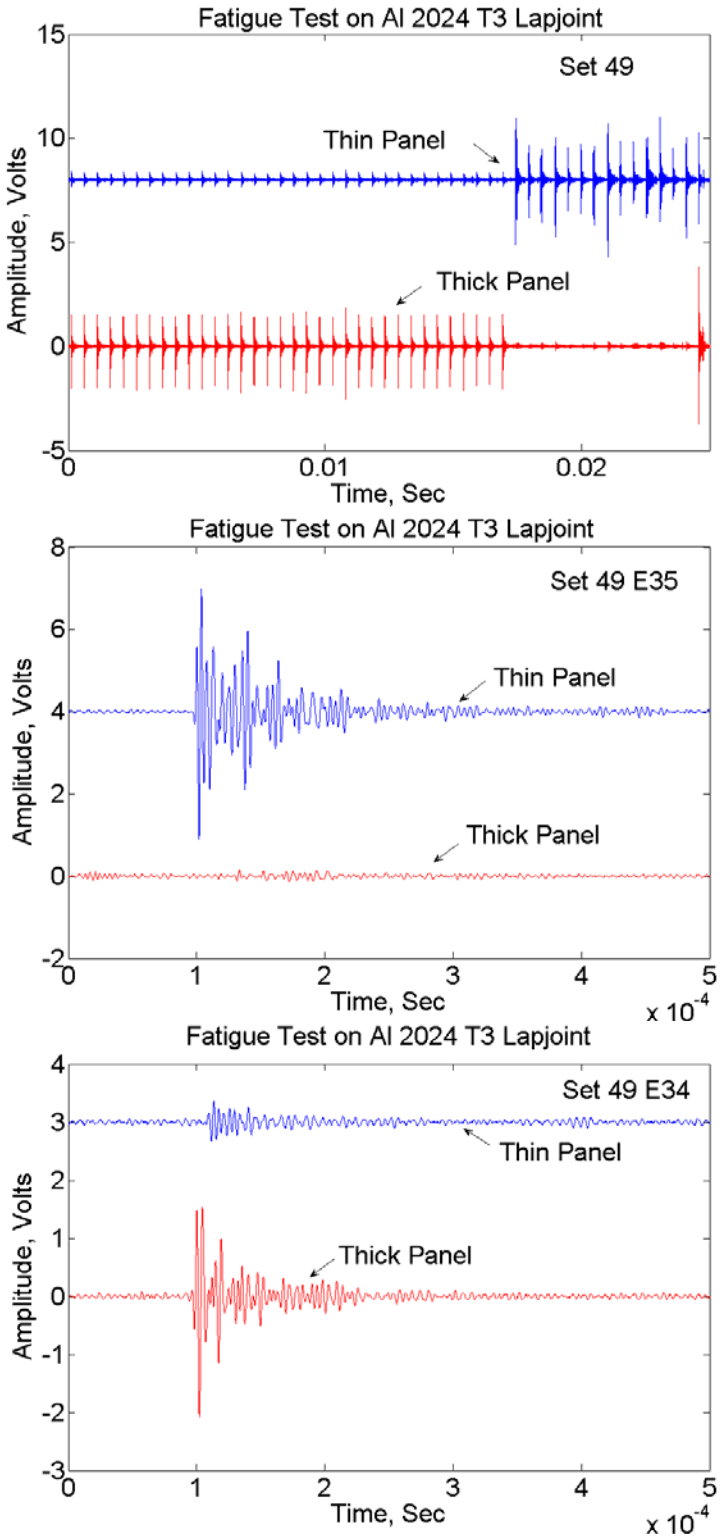

Figure 23. (a) A sequence of AE events recorded towards the end of the seventh segment of fatigue load and (b) one of these events magnified along the time axis for which the top continuous sensor received the emissions first; (c) one of the events for which the bottom continuous sensor received the signal first.

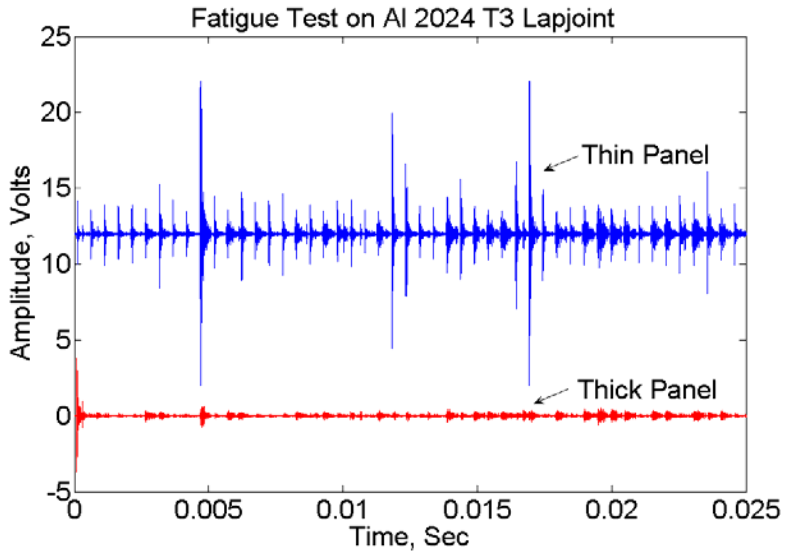

(a)

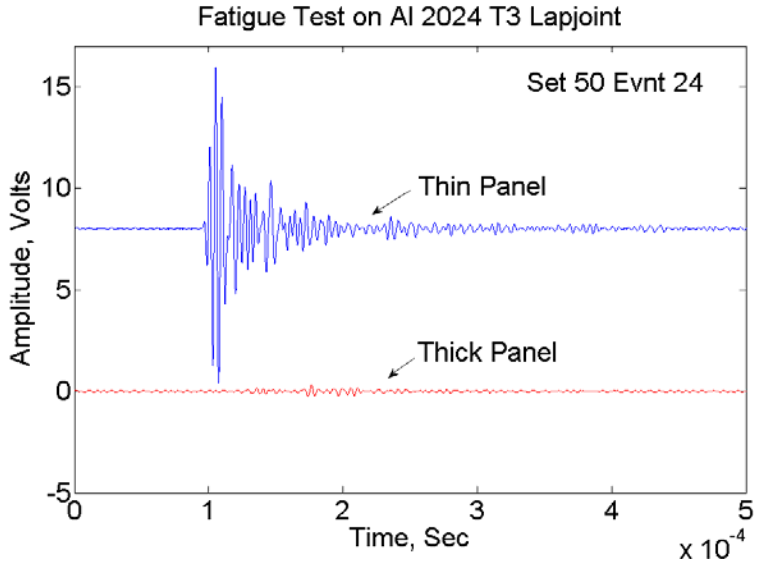

(b)

Figure 24. (a) A sequence of AE events recorded towards the end of the seventh segment of fatigue load and (b) one of these events magnified along the time axis.

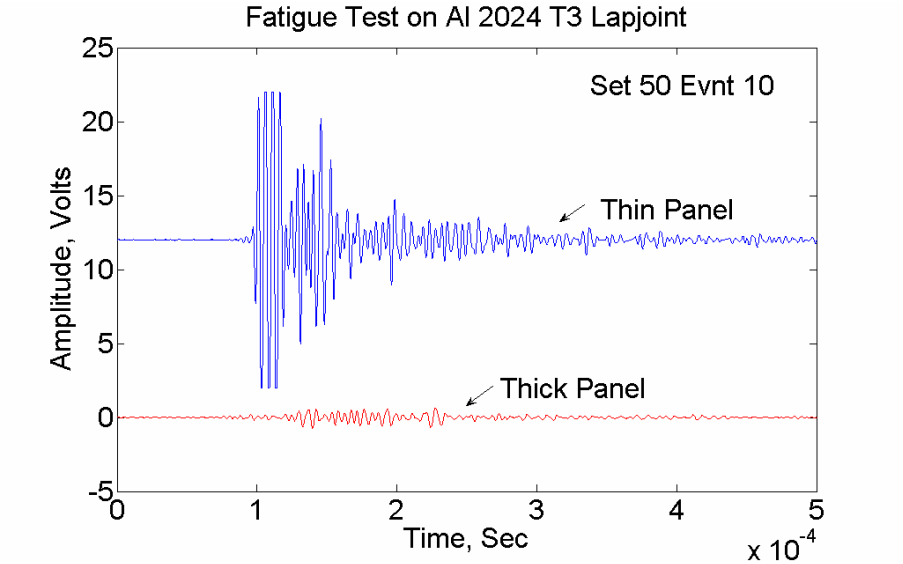

(c)

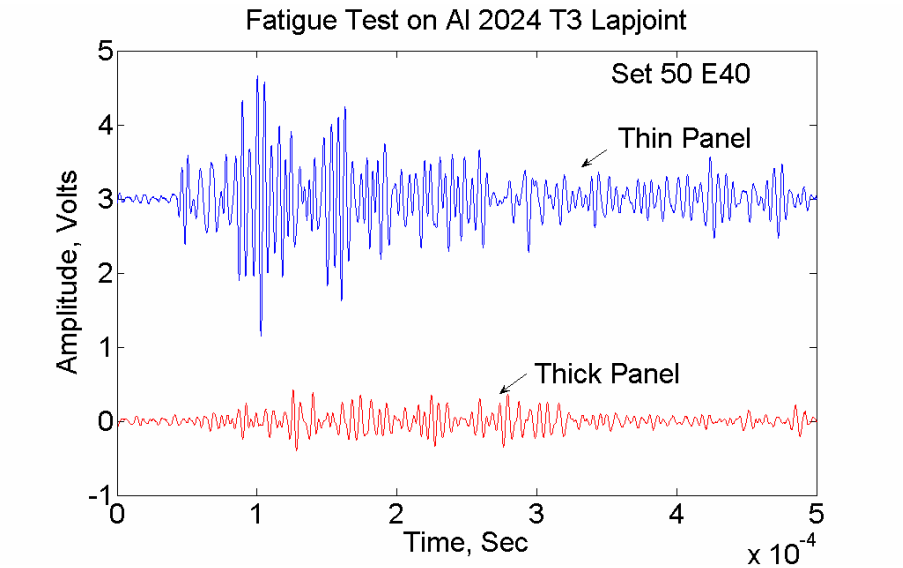

(d)

Figure 24. (c) One of the events from the sequenced shown above which had very high energy indicating fast crack growth; (d) another event in this sequence with long rise time and long duration.

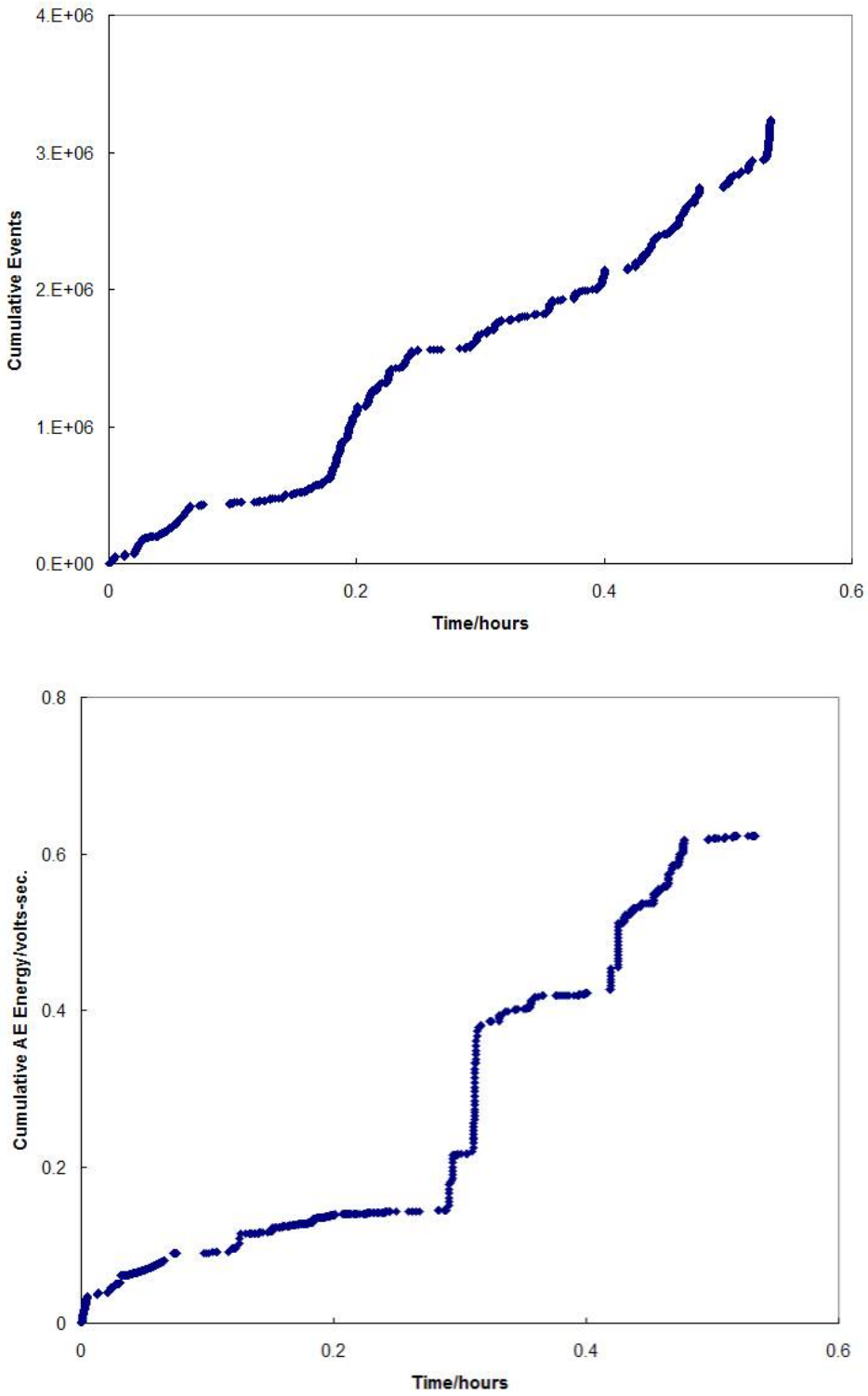

Figure 24. (a) Cumulative acoustic emission events recorded during the seventh segment of the fatigue loading as a function of time; (b) cumulative acoustic emission energy as a function of time, for the lap joint specimen extracted from KC-135 fuselage.

10.0 SUMMARY

The application of acoustic emission technique for monitoring fatigue crack growth in aluminum fuselage lap joints are described in this paper. Continuous sensor is evaluated for this application. A large number of tests were used for gaining an understanding of the acoustic emission behavior from 7075-T6 and 2024-T3 materials. The continuous sensor was found to perform satisfactorily for detecting crack growth rates of the order of 0.001 mm per cycle in flat panel specimens. Test on the lap joint extracted from the KC-135 fuselage provided the most encouraging results. The failure in the top grip area was detected before the failure. In addition, from the signals recorded also indicated the presence of crack growth at the lower row of rivets in the bottom half of the lap joint. In conclusion, the continuous sensor appears to be a viable solution for monitoring crack growth in aging aircraft application.

ACKNOWLEDGEMENT

Air Force Research Laboratory, Materials Directorate, supported this work. This support is gratefully acknowledged. Authors would also like to thank the Dean of Engineering for providing additional funding to perform the supporting work for this contract.

11.0 REFERENCES

1. M.J. Sundaresan, A., Ghoshal, M.J., Schulz, "A Continuous Sensor to Measure Acoustic Waves in Plates," Journal of Intelligent Material Systems and Structures, Vol. 12, No.1, pp.41-56, January 2001.

2. M. J. Sundaresan, A. Ghoshal, and M.J. Schulz, “Continuous Acoustic Emission and Vibration Sensor,” U.S. Patent number 6,399,939.

3. D.O. Harris and A.S. Tetelman, “Detection of Fatigue Crack Growth by Acoustic Emission Techniques" Materials Evaluation, Vol. 28, No. 10, pp. 221-227; 1970.

4. D.O. Harris, “Continuous Monitoring of Fatigue Crack Growth by Acoustic Emission Methods”, Experimental Mechanics, Vol. 14, No. 2, pp. 71-81, February 1974.

5. I. Searle, S. Ziola, P. Rutherford, “Crack Detection in Lap-Joints using Acoustic Emission,” Proceedings SPIE Volume 2444, pp.212-223, 1995.

6. M. J. Sundaresan, G. Grandhi, L. Uitenham, M. J. Schulz, J. Kemerling, D. Hughes, “Development of an Acoustic Emission Based Structural Health Monitoring System,” Fourth International Workshop on Structural Health Monitoring, September 15-17, Stanford University, CA, 2003.

APPENDIX 1: USAGE OF THE NATIONAL INSTRUMENT LABVIEW BASED SOFTWARE FOR ACOUSTIC EMISSION DATA COLLECTION

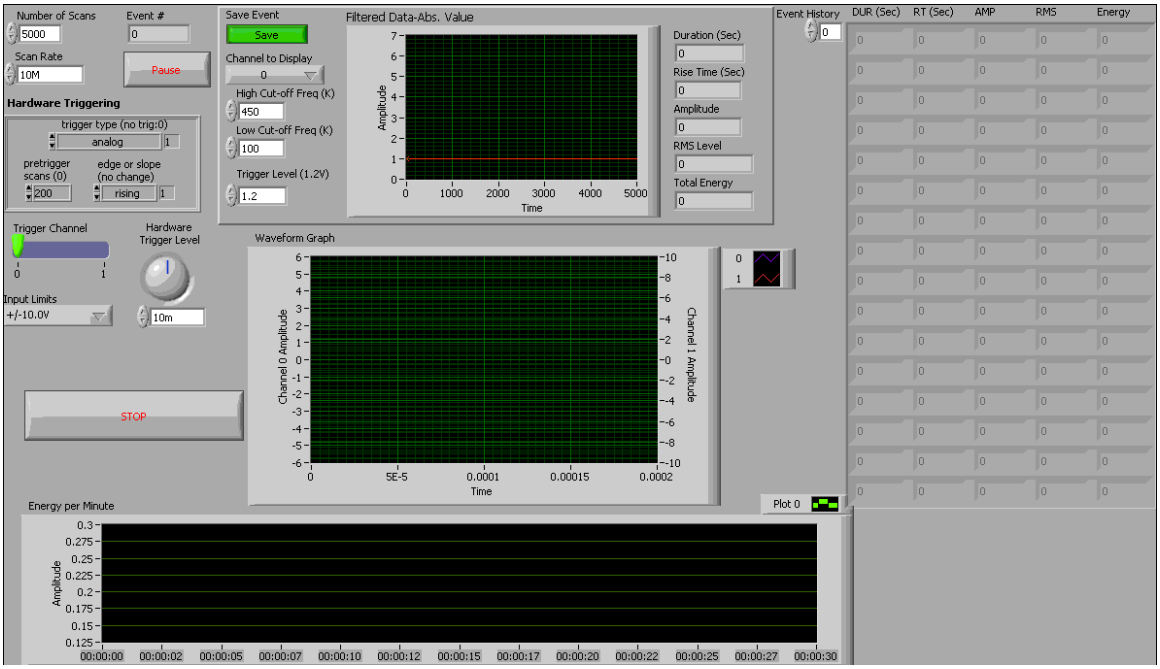

Figure A1. The front panel of the LabView vi code

The front panel of the LabView vi code written by Triad Semiconductor for NC A&T SU is shown in Figure A1. The functioning of this software is similar to a digital oscilloscope. This software is set up to acquire two channels of acoustic emission data, process each of the waveforms in near real time, and tabulate the individual event parameters such as event duration, rise time, amplitude, rms voltage and energy, in the form of a scrolling table on the right side of the front panel. The individual event waveforms corresponding to the two channels are displayed in the center of the front panel. This waveform display is helpful for deciding the selection of the voltage level used to record the events and to set the threshold level. In addition, the cumulative acoustic emission energy determined for each minute is displayed as a moving bar chart at the bottom of the screen. This cumulative energy released per minute is related to the crack growth rate. For faster crack growth rates, higher energy will be released.

The functions such as sampling rate, duration of event, trigger level, trigger source, pre-trigger duration, and the voltage amplitudes are selectable from the drop down menus in the top left of the front panel. The threshold level in the hardware trigger level icon shown is changed depending on crack growth rate. For slower rates, crack signals will be smaller amplitude and hence threshold will be small. The channel which is to be triggered can be changed in the "Trigger Channel" icon. Pre-trigger scan gives the number of samples delayed before the signal crosses the threshold. The software filters used for processing the acoustic emission signals are selectable from the menus for 'High Cut-off freq (K)' and 'Low Cut-Off Freq (K)'. The filters to be used will depend on type of signals appeared. Typical crack signals will be in having frequency range of 100-500 kHz and hence filters will be used accordingly. The vi is started using the right arrow in the top of the menu. The data is recorded as two separate files. The first is designed to record 50 individual AE events for each file. The user is prompted to chose the file name and directory information when the right arrow button is pressed. The second file is the tabular record of the AE parameters shown in the right side of the screen. The data acquisition can be paused and resumed by successively pressing the 'Pause' button. To terminate the data acquisition, one needs to use the 'STOP' button. It is to be noted that the use of the LabView's stop button instead of the 'STOP' button near the bottom of the front panel may lead to loss of data.